IEEE Control Systems Letters paper presented at
2023 62nd IEEE Conference on Decision and Control (CDC)
December 13-15, 2023. Marina Bay Sands, Singapore

# Robust Control of Cascaded H-Bridge Multilevel Inverters for Grid-Tied PV Systems Subject to Faulty Conditions

Hanane Katir*,[1], Abdelmajid Abouloifa[1], Elhoussin Elbouchikhi[2],
Afef Fekih[3], Karim Noussi[1] and Abdelali El Aroudi[4]

***Abstract*— This paper deals with the design and implementation of a robust control approach for grid-tied PV systems. The main controller's objectives are to inject the maximum available power to the grid, whilst guaranteeing power quality even under faulty conditions. To this end, a multi-loop regulator is designed for the Cascaded H-Bridge Multilevel Inverters (CHBMIs) by combining a sliding mode control strategy for maximum power point tracking and a Lyapunov approach for Power Factor Correction (PFC). Validation of the proposed approach using Matlab/ SimPowerSimscape environment confirmed the ability of the proposed approach to successfully accomplish its objectives in terms of references tracking and regulation under both matching and mismatching irradiation levels as well as faulty modes stemming from the photovoltaic (PV) panels and/or the dc-dc converters. Additionally, the proposed approach was shown to outperform conventional approaches and enable the continuous operation of the PV system under various failure modes affecting multiple PV panels and/or their associated dc-dc boost converters.**

***Index Terms*— Cascaded H-Bridge Multilevel Inverters, Fault Tolerance, Lyapunov Tools, Photovoltaic Energy, Sliding Mode Control.**

## I. Introduction

DUE to the proliferation of Nonlinear Loads (NLs) in numerous industrial applications and their negative effects on the grid, Active Power Filters (APFs) have been proposed as a solution to eliminate the total reactive and harmonics powers. In fact, they provide the system with these powers in equal quantities in order to improve the grid power factor and power quality. These systems are considered as current source inverters operating in parallel with the grid and the NLs [1].

Multilevel APFs have proven powerful performance, especially when combined with renewable energies making them aligned with the worldwide energetic transition towards clean energies. Thanks to their scalability, CHBMIs have been considered to maximize the efficiency of APFs [2]-[5]. However, designing controllers for such multilevel systems is a very challenging task. Additionally, the system's nonlinearities and presence of unstable zero dynamics on the dc link side of the grid further complicate this task.

In fact, PI-based control methods are widely investigated for the control of CHBMIs [6]. However, it is well known that PI controllers are not robust against uncertainties, external disturbances, and un-modeled dynamics. Furthermore, they lead to remarkable undesired oscillations in the dc link voltage, active and reactive powers during faulty conditions, thereby increasing the total harmonics of the output [7]-[8]. Backstepping approaches were shown to be effective in controlling CHBMIs as presented in [9]. However, this method lacks robustness, i.e., any change in the components' values led by aging, for example, would degrade the system performance. Sliding mode control has recently emerged as one of the most effective robust control techniques for nonlinear and uncertain systems [10]-[11]. The controller is designed to drive and then constrain the system states to lie within a neighborhood of the switching manifold and become insensitive to a class of uncertainties [12].

To overcome the aforementioned problems, we propose in this paper a sliding mode control-based approach for the CHBMIs of a grid-tied PV system. This study focuses on:

- The design of a multi-loop regulator for the CHBMIs by combining a sliding mode control strategy for maximum power point tracking and a Lyapunov approach for PFC.
- A control design that enables the CHBMI system to acts as a filter to compensate for the load harmonics and reactive powers, whilst at the same time generating active power to supply both the power grid and NLs.
- A fault tolerant control approach capable of ensuring good performance in the presence of both matching and mismatching irradiation levels, as well as faulty modes stemming from the PV panels and/or the dc-dc converters.

*Corresponding author: Hanane Katir
**Abdelali El Aroudi acknowledges the support and funding of the Spanish Ministerio de Ciencia e Innovación under Grant PID2020-120151RB-I00.
[1]Hanane Katir, Abdelmajid Abouloifa and Karim Noussi are with ESE Laboratory, ENSEM of Casablanca, Hassan II University of Casablanca, Morocco. katir.hanane@gmail.com; abdelmajid.abouloifa@etu.univh2c.ma; karim.noussi2@gmail.com
[2]Elhoussin Elbouchikhi is with ISEN Yncrea Ouest, LABISEN, Nantes Campus, 33Q, Avenue du Champ de Manoeuvre, 44470, Carquefou, France. elhoussin.elbouchikhi@isen-ouest.yncrea.fr
[3] Afef Fekih is with Department of Electrical and Computer Engineering, University of Louisiana at Lafayette, Lafayette, LA 70504, USA. afef.fekih@louisiana.edu
[4]Abdelali El Aroudi is with Universitat Rovira i Virgili, Department d'Enginyeria Electrònica Elèctrica i Automàtica, Tarragona, Spain. abdelali.elaroudi@urv.cat

The remainder of this paper is organized as follows. Section II represents the system description and modeling. Section III details the proposed controller design. Section IV highlights the simulation results. Conclusions are drawn in section V.

## II. System Description and Modeling

### A. System Description

This paper focuses on the study of a PV-shunt APF based on a double stage conversion chain. The first stage includes $N$ dc-dc boost converters linked to $N$ PV generators. The second one involves a CHBMI connected in parallel to the association of NLs and power grid through a filtering inductance. The schematic diagram representing the aforementioned system is shown in Fig. 1. The CHBMI contains $N$ H-bridge converters, which leads to strengthening the filtering abilities of the system and thus making the grid current smoother. The major reason behind using this structure is the reduced dimensions of the passive filter at the output and the distribution of stress on the switching devices. Additionally, it can operate under faulty modes tolerating failures that may take place in the PV sources and/or the dc-dc boost choppers.

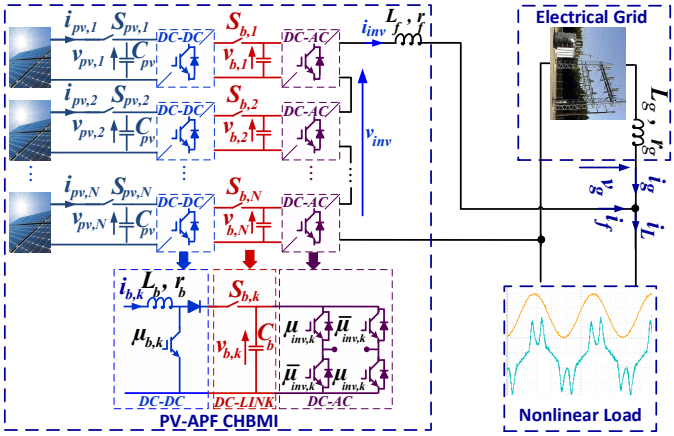


Fig. 1. PV-APF conversion chain structure.

### B. Switched Mathematical Model

The entire conversion chain, Fig. 1, can be mathematically described using Kirchoff's laws. This system can be divided into three subsystems in accordance with the control objectives. The first one (1) is meant to achieve the Maximum Power Point Tracking (MPPT) requirement; whereas, the second one (2) regulates the dc link voltage, and the third one (3) is intended to perform the power factor correction on the grid side.

$$C_{pv}\frac{dv_{pv,k}}{dt} = i_{pv,k} - i_{b,k}, \tag{1a}$$

$$L_b\frac{di_{b,k}}{dt} = -r_b i_{b,k} + v_{pv,k} - (1-\mu_{b,k})v_{b,k}, \tag{1b}$$

$$L_f\frac{di_f}{dt} = -r_f i_f + \sum_{k=1}^{N}\mu_{inv,k}v_{b,k} - v_g, \tag{2}$$

$$C_b\frac{dv_{b,k}}{dt} = (1-\mu_{b,k})i_{b,k} - \mu_{inv,k}i_f, \tag{3}$$

where $k = 1, 2, ..., N$, $v_{pv,k}$ and $i_{pv,k}$ are the voltage and current of the $k^{th}$ PV generator. $v_{b,k}$ and $i_{b,k}$ are the voltage and current of the $k^{th}$ dc-dc boost converter. $v_g$ and $i_g$ denote the grid voltage and current. $v_{inv}$ represents the CHBMI voltage. $i_f$ is the current of the APF. $\mu_{inv,k} \in \{-1, 1\}$ and $\mu_{b,k} \in \{0, 1\}$ are the switching functions of the $k^{th}$ H-bridge inverter and the $k^{th}$ dc-dc boost converter, respectively.

### C. Average Mathematical Model

The averaged model related to the switched mathematical formalism can be described as follows [12].

$$C_{pv}\dot{x}_{1,k} = i_{pv,k} - x_{2,k}, \tag{4a}$$

$$L_b\dot{x}_{2,k} = -r_b x_{2,k} + x_{1,k} - (1-u_{b,k})x_{4,k}, \tag{4b}$$

$$L_f\dot{x}_3 = -r_f x_3 + \sum_{k=1}^{N}u_{inv,k}x_{4,k} - v_g, \tag{5}$$

$$C_b\dot{x}_{4,k} = (1-u_{b,k})x_{2,k} - u_{inv,k}x_3, \tag{6}$$

where, $k = 1, \ldots, N$ and the quantities $x_{1,k}$, $x_{2,k}$, $x_3$, $x_{4,k}$, $u_{inv,k}$ and $u_{b,k}$ are the average values over the switching period $T_s$ of the signals $v_{pv,k}$, $i_{b,k}$, $i_f$, $v_{b,k}$, $\mu_{inv,k}$ and $\mu_{b,k}$, respectively.

The aforementioned average model describes a nonlinear system of $3N + 1$ order with unstable zero dynamics with respect to the dc link voltages $x_{4,k}$. Consequently, this latter cannot be directly controlled. It would need to go through the regulation of the filter current $x_3$ first.

## III. Controller Design

### A. Control Objectives

This study has been performed on the comprehensive system depicted in Fig. 1. The control design aims to fulfill the following multifold objectives, under both, regular and faulty modes.

- MPPT objective: The $k^{th}$ PV voltage, $v_{pv,k}$, must match its reference, $v^*_{pv,k}$, which corresponds to the Maximum Power Point (MPP). From a control perspective, the weighted error $e_{1,k} = C_{pv}(v_{pv,k} - v^*_{pv,k})$ must be regulated to zero as a result of the synthesis of the binary control signal $\mu_{b,k}$ in the switched model.
- PFC objective: The filter current, $i_f$, is aimed to tightly track its reference, $i^*_f = i_L - \beta v_g (\beta \in \mathbb{R})$, in a way that the NLs reactive and harmonics powers are compensated by appropriately designing the control law $u_{inv,k}$, which is calculated based the average model.
- The dc link voltage regulation: The sum of dc link voltages, $v_b$, are regulated to a desired value, $v^*_b$, by acting on the intermediate signal $\beta$.

To meet the design specifications, we consider a multi-loop regulator that combines the robust properties of sliding mode control with the stability properties of the Lyapunov theory. Our first concern begins with ensuring that the PV sources function at their MPPs. To accomplish this objective, an MPPT algorithm must be used to generate the reference, which corresponds to the MPP PV voltage. This reference is utilized by the controller as a roadmap to regulate the voltage

across each photovoltaic source individually given the nature of the CHBMI that requires having independent dc inputs. We also desire to control the grid current to meet a unitary power factor requirement via the inner loop of a cascaded regulator. The outer loop manages the dc link voltages via a filtered PI regulator, in a way that they provide dc voltages to the CHBMI. Figure 2 represents the schematic diagram of the regulator.

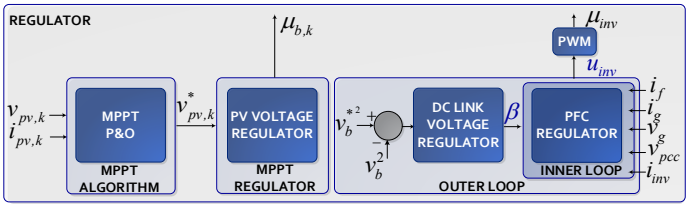


Fig. 2. Regulator structure.

### B. MPPT objective: PV voltage regulator design

At this stage, we intend to design a control law $\mu_{b,k}$ to force the $k^{th}$ PV voltage to match its reference generated by the $k^{th}$ MPPT block. A sliding mode control approach will be used to allow reaching and maintaining the system on a suitable sliding manifold [13]. The synthesis of the control law calls first for defining the $k^{th}$ weighted error between the PV voltage and its reference as follows.

$$e_{1,\,k} = C_{pv}\left(v_{pv,\,k} - v^{*}_{pv,\,k}\right), \tag{7}$$

Using (1a) and supposing that the $k^{th}$ PV reference voltage, $v^{*}_{pv,k}$, is quasi-stationary, the time derivative of the $k^{th}$ weighted error is:

$$\dot{e}_{1,\,k} = i_{pv,\,k} - i_{b,\,k}, \tag{8}$$

Let us consider the following general form of the switching function enabling the stabilization of the first subsystem [13]:

$$S_k\left(e_{1,k}\right) = \left(\frac{d}{dt} + \alpha_1\right)^{n_{b,k}-1} e_{1,k}\ , \tag{9}$$

where, $\alpha_1$ is a positive design parameter and $n_{b,\,k}$ is the relative degree of the system to be controlled.
Since $n_{b,\,k} = 2$ and using equations (8) and (9), the switching function turns into:

$$S_k\left(e_{1,\,k}\right) = i_{pv,\,k} - i_{b,\,k} + C_{pv}\alpha_1\left(v_{pv,\,k} - v^{*}_{pv,\,k}\right) \tag{10}$$

The time derivative of the switching function can be expressed therefore as follows:

$$\dot{S}_k\left(e_{1,k}\right) = \frac{di_{pv,k}}{dt} + \frac{r_b}{L_b}i_{b,k} - \frac{v_{pv,k}}{L_b} + \frac{1-\mu_{b,k}}{L_b}v_{b,k} + C_{pv}\alpha_1\dot{v}_{pv,k} \tag{11}$$

The equivalent control under ideal sliding mode motion can be obtained by using the invariance condition $\dot{S}_1\left(e_{1,\,k}\right) = 0$. As a result, one finds:

$$\mu^{eq}_{b,k} = 1 + \frac{L_b(\frac{di_{pv,k}}{dt} + C_{pv}\alpha_1\dot{v}_{pv,k}) + r_b i_{b,k} - v_{pv,k}}{v_{b,k}} \tag{12}$$

To deduce the discontinuous control law, we use the reaching condition $\dot{S}_k\left(e_{1,\,k}\right)S_k\left(e_{1,\,k}\right) < 0$. The switching policy has to combine the ON and OFF dynamics of the dc-dc boost converter to create a trajectory that slides on average along the surface $\Sigma_k := \{x | S_k(e_{1,k} = 0)\}$. The ideal sliding behavior is therefore characterized by an undesired infinite switching frequency. To mitigate this problem, a hysteresis window is introduced around the sliding surface. By adding this hysteresis window, the control law inside the hysteresis window becomes as follows.

$$\mu_{b,k} = \begin{cases} 0, & \text{if, } S_k(e_{1,k}) > +h \\ 1, & \text{if, } S_k(e_{1,k}) < -h \end{cases} \tag{13}$$

while inside this window $\mu_{b,k}$ maintains its previous value when the last switching has taken place, where $h$ is the amplitude of the hystresis width.

### C. PFC Controller design

In this subsection, a PFC controller is designed, based on the averaged model, in order to compensate for the reactive and harmonics powers of the NL. This regulator acts on the APF current so as to get a sinusoidal grid current ($i_g = \beta v_g$) in phase or out of phase with the grid voltage $v_g = \sqrt{2}V_g\sin\left(\omega_g t\right)$. This inner loop controller is a part of a cascaded regulator whose outer loop regulates the dc link voltages by adjusting the intermediate signal $\beta$.
Let us define the following tracking error between the APF current $x_3$ and the desired reference $x^{*}_3 = i_L - \beta v_g$:

$$e_f = L_f\left(x_3 - x^{*}_3\right) \tag{14}$$

Using equation (5), time derivation of the above defined tracking error is given as:

$$\dot{e}_f = -r_f x_3 + \sum_{k=1}^{N} u_{inv,k}x_{4,k} - v_g - L_f\dot{x}^{*}_3 \tag{15}$$

If we choose the control laws $u_{inv,k}$ so that:

$$\sum_{k=1}^{N} u_{inv,k}x_{4,k} = -\lambda_f e_f + r_f x_3 + v_g + L_f\dot{x}^{*}_3 \tag{16}$$

$\lambda_f$ is a positive design parameter that fixes the error convergence dynamics.
Therefore, the system (15) will be exponentially stable with respect to the following Lyapunov candidate function:

$$V_f = 0.5\,e_f^2 \tag{17}$$

The derivative of the chosen Lyapunov candidate function is:

$$\dot{V}_f = e_f\dot{e}_f = -\lambda_f e_f^2 \tag{18}$$

The evolution of the tracking error $e_f$ is given as:

$$e_f\left(t\right) = e_f\left(0\right)e^{-\lambda_f t} \tag{19}$$

***Remark 1:*** If we consider that all the H-bridge inverters are similarly controlled ($u_{inv,k} = u_{inv}, \forall k = 1,\ldots,N$), then the derived control laws (16) can be reduced to:

$$u_{inv} = \left(\sum_{k=1}^{N} x_{4,k}\right)^{-1}\left(-\lambda_f e_f + r_f x_3 + v_g + L_f\dot{x}^{*}_3\right) \tag{20}$$

### D. Design of the dc link voltage regulator

*1) Relationship between the dc link voltage and $\beta$ :* For the sake of proper operation of the CHBMI, it is necessary to regulate its input voltages to a fixed value, $v_b^*$, respecting the following constraint:

$$v_b^* > V_g/N \tag{21}$$

For this reason, it is compulsory to establish the relationship between the dc link voltages and the input signal $\beta$.

***Lemma-*** Consider the system presented in Fig 1, described by its average mathematical model in (4)-(6), in closed-loop with the developed controller consisting of the MPPT and PFC regulators (12) and (20), if the following conditions (i and ii) are verified,

i. The outer loop is designed to have slower dynamics than the MPPT and PFC loops;

ii. The parameters $L_g$, $r_g$, $L_b$, $r_b$, $L_f$ and $r_f$ are sufficiently small and can be neglected.

Then, the relationship between the dc link voltages and the input signal $\beta$ is given by the following expression:

$$\frac{C_b}{2}\dot{y}\left(t\right) = p_{PV}\left(t\right) - p_L\left(t\right) + p_g\left(t\right), \tag{22}$$

where $p_{PV}\left(t\right) = \sum_{k=1}^{N} v_{pv,k} i_{b,k}$, $p_L\left(t\right) = v_g i_L$ and $p_g\left(t\right) = \beta v_g^2$ represent the instantaneous powers of the PV, NL and grid sides, and $y = \sum_{k=1}^{N} x_{4,k}^2$.

***Note***- Equation (22) represents the mathematical model to be used in order to regulate the dc link voltages ($y$) by acting on the control signal $\beta$ and using the averaged model.

***Proof-*** To prove equation (22), let us first deduce the reduced averaged form of the control laws $u_{b,k}^{eq}$ and $u_{inv}$ with respect to the previous hypothesises. Knowing that the errors $e_{1,k}$ and $e_f$ vanish fast, the signals $x_{1,k}$ and $x_3$ rapidly match their references $x_{1,k}^*$ and $x_3^*$, respectively.
Consequently, equations (12) and (20) turn into:

$$u_{b,k}^{eq} \simeq 1 - \frac{x_{1,k}}{x_{4,k}} \tag{23}$$

$$u_{inv} \simeq v_g/v_b \tag{24}$$

Plugging (23) and (24), equations (6) become:

$$C_b \dot{x}_{4,k} = \frac{x_{1,k}}{x_{4,k}} x_{2,k} - \frac{v_g}{\sum_{k=1}^{N} x_{4,k}} \left(i_L - \beta v_g\right) \tag{25}$$

Rearranging the above equations lead to:

$$\frac{C_b}{2}\dot{x}_{4,k}^2 = x_{1,k}x_{2,k} - \frac{v_g}{\sum_{k=1}^{N} x_{4,k}} x_{4,k}\left(i_L - \beta v_g\right) \tag{26}$$

Summing equations (26) from $k=1$ to $k=N$, one gets:

$$\frac{C_b}{2}\sum_{k=1}^{N}\dot{x}_{4,k}^2 = \sum_{k=1}^{N} x_{1,k}x_{2,k} - v_g\left(i_L - \beta v_g\right) \tag{27}$$

The above equation can be reformulated, such as :

$$\frac{C_b}{2}\dot{y}\left(t\right) = p_{PV}\left(t\right) - p_L\left(t\right) + \beta v_g^2 \tag{28}$$

It is worth noting that this formula physically reflects the instantaneous power conservation principle.

***Remark 2:*** It is worth mentioning that the quantity on the right side of equation (28) has ripples of an angular frequency of $2\omega_g$, in addition to the dc component that represents the active power. These ripples will always exist independently of any used regulator type. Therefore, the dc link regulator can only be designed based on the averaged model, over half of the grid period, which is given as:

$$\frac{C_b}{2}\dot{\bar{y}} = \bar{p}_{PV} - \bar{p}_L + V_g^2\bar{\beta}\left(t\right) \tag{29}$$

where, $\dot{\bar{y}}$, $\bar{p}_{PV}$ and $\bar{p}_L$ are the averaged values of $\dot{y}$, $p_{PV}\left(t\right)$ and $p_L\left(t\right)$, respectively.

*2) The Control Signal $\beta$ :* If the signal $\beta$ is chosen as:

$$\beta\left(t\right) = \frac{K_p\left(y^* - y\right) + K_i\int\left(y^* - y\right)dt + p_L\left(t\right) - p_{PV}\left(t\right)}{V_g^2} \tag{30}$$

Then, the closed loop system will be described by its transfer function, given as:

$$\frac{Y\left(s\right)}{Y^*\left(s\right)} = \frac{1 + \frac{2\zeta}{\omega_0}s}{1 + \frac{2\zeta}{\omega_0}s + \frac{s^2}{\omega_0^2}} \tag{31}$$

where, $\zeta$ and $\omega_0$ are the desired damping factor and the natural frequency. Their values are fixed by the appropriate tuning of the design parameters $K_p$ and $K_i$, given as:

$$K_p = \zeta C_b \omega_0 \tag{32}$$

$$K_i = 0.5 C_b \omega_0^2 \tag{33}$$

## IV. Simulation Results

This section is dedicated to the simulation of the proposed PV-fed double stage system in order to demonstrate the designed APF efficacity to compensate for the reactive and harmonic powers. Since the CHBMI-APF is powered by PV panels, it is able to generate active power designated to be consumed by the NLs and the surplus could be injected to the electrical grid. Another point to put under test is the capacity of the controlled system to cope with defective conditions thanks to its modularity. The simulation is carried out in Matlab/SimPowerSystems using the system and regulator parameters listed in Table I.

TABLE I
PLANT SYSTEM AND REGULATOR PARAMETERS

| Parameters | Symbols | Values |
|---|---|---|
| Power grid | $V_g, \omega_g,$ | 230 V , 100$\pi$rad/s, |
| | $L_g, r_g$ | 0.2 mH, 0.5 m$\Omega$ |
| Boost choppers | $C_{pv}, L_b, r_b$ | 0.2 mF, 3 mH, 50 m$\Omega$ |
| Capacitors of the dc link | $C_b$ | 2 mF |
| APF | $L_f, r_f$ | 0.5 mH, 50 m$\Omega$ |
| PV voltage regulator | $\alpha_1, \alpha_2$ | 1000, 6667 |
| Grid current regulator | $\lambda_f$ | 1000 |
| Regulator of the dc link | $K_p, K_i$ | 0.04, 0.004 |

For simulation purposes, we consider a limited version of Fig. 1-system ($N = 3$), consisting of three independent PV arrays (1Soltech 1STH-215-P) each with four parallel strings and two series-connected modules. Each of the PV panels provides active power to a dc-dc boost converter coupled with a dc link that supplies an H-bridge cell. On the ac side, there is a CHBMI comprising three H-bridge inverters connected in series and linked on their turns to the point of common coupling via an $L$-filter, aiming at delivering active, reactive and harmonics powers to the NLs-grid association.

The simulation results are based on the following testing protocol:

**Mode 1 - [0, 0.5 s]:** All PV sources operate with an irradiation of (1000 W/m$^2$). It is expected that the active power delivered by the studied system is more than the one required by the NL. Therefore, the PV-APF feeds the NLs and injects the surplus power to the electrical grid.

**Mode 2 - [0.5 s, 1 s]:** PV$_1$ (600 W/m$^2$), PV$_2$ (800 W/m$^2$) and PV$_3$ (700 W/m$^2$). During this mode, the PV panels of the APF are working under mismatching irradiations to prove the efficacity of the system in real non ideal conditions where, the PV panels usually operate under different irradiations for multiple reasons, such as shading, non-uniform aging of the PV cells, etc. It is worth noting that these specifications would lead to an active power generation corresponding approximately to the one required by the NLs. Therefore, the PV-APF only feeds the NLs; whereas, the electrical grid does not provide any power to this latter. It actually receives the small amount of the surplus power.

**Mode 3 - [1 s, 1.5 s]:** PV$_1$ (defective/disconnected), PV$_2$ (800 W/m$^2$) and PV$_3$ (700 W/m$^2$). During this mode, the system faces faulty conditions causing one PV source and/or dc-dc boost converter to malfunction or get disconnected. Thus, one of the H-bridge cells is not powered by its corresponding dc source. This failure prohibits the PV panels of the APF from providing the necessary power to the NLs. Thus, the main grid supplies the rest of the active power.

**Mode 4 - [1.5 s, 2 s]:** PV$_1$ and PV$_2$ (defective/disconnected), and PV$_3$ (700 W/m$^2$). During this mode, the system is tested under severe faulty conditions causing two of its three PV sources and/or dc-dc boost converters to fail or get disconnected. At this point, there is only one PV source providing power to the system that partially feeds the NLs. The main grid delivers the rest of power required by the NLs.

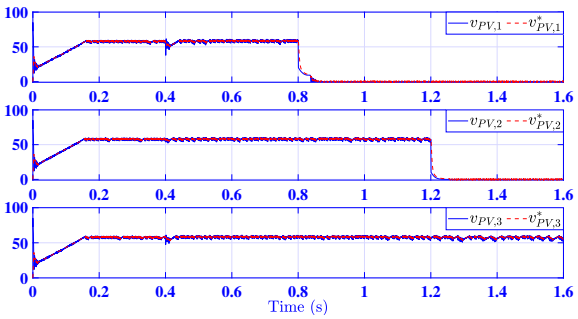


Fig. 3. PV voltages and their references.

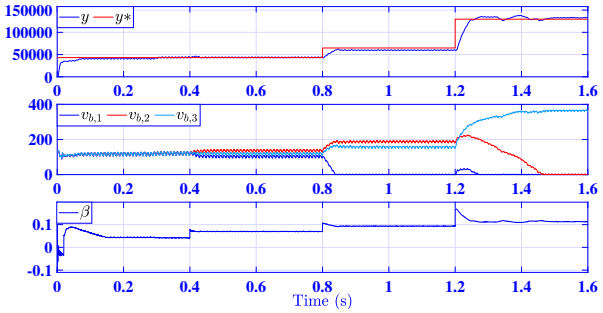


Fig. 4. The regulation of the dc link and the control input $\beta$.

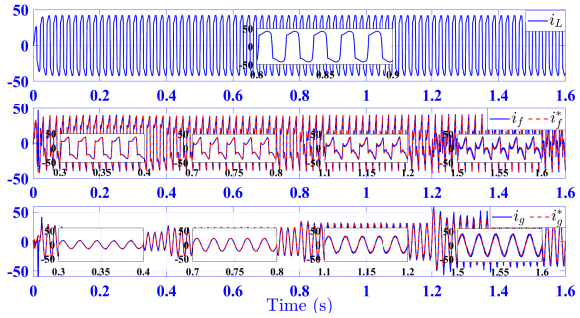


Fig. 5. Nonlinear load, filter and grid currents.

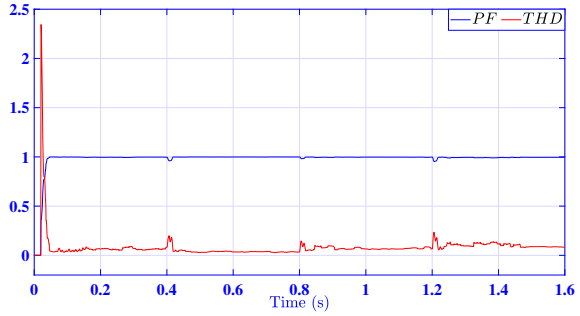


Fig. 6. The Power Factor (PF) and the Total Harmonic Distortion (THD) of the grid current.

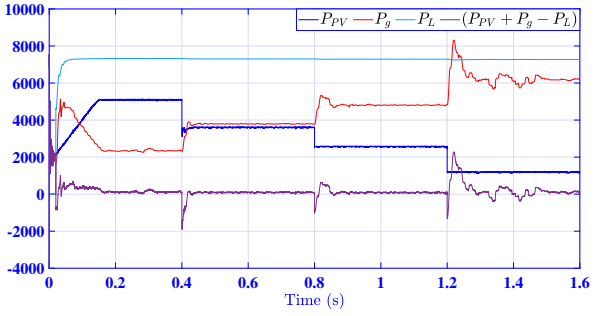


Fig. 7. PV, grid, NLs powers, and power conservation check.

With respect to the suggested protocol and the irradiance changes profile, the controlled system has proven its ability to reach the desired objectives, in terms of the MPPT requirements as it could be seen in Fig. 3. This latter draws the

attention to the individual PV voltage tracking of the reference provided by the Perturb and Observe (P&O) algorithm [14]. As for the dc link voltage regulation, Fig. 4 demonstrates the achievement of this objective even within different occurring changes. It illustrates the regulation of the dc link voltage to its desired reference, which varies according to the number, $N_o$, of well-operating H-bridge inverters, given by:

$$y^* = \frac{360^2}{N_o} \tag{34}$$

This figure also shows the behavior of the individual dc link voltages across each capacitor. As it could be noticed, the regulation of the dc link voltages allows the system to operate in the failure mode where its sources might be subject to disconnection or complete failure, provided that at least one of them generates power. This feature is the one causing the capacitors to reach the equilibrium when the PV panels are working under the same standard test conditions. Otherwise, each capacitor progresses in a way forcing $y$ to match its reference. In the case of losing the two power sources, the left capacitor is the only one enabling the fulfilment of this control objective. The control law $\beta$ given by the PI regulator is depicted in this figure too. This signal is bounded and correlates with the grid current magnitude, the grid power, and the PV irradiations. The NL current is found in Fig. 5. Its FFT analysis shows that it has a THD of 31.68%. The output filter's current of this controlled system must efficiently match its reference generated by the PI regulator to ensure lowering the THD percentage of the grid current. As seen in the same figure, the filter's current tightly tracks its reference in all modes. Consequently, the grid current is sinusoidal and in phase, or out of phase, with the grid voltage resulting in the achievement of the PFC requirement, as seen in Fig. 6, where the THD is less than 5% and the power factor is unitary. An FFT analysis has been performed over the grid current to precisely check the compensation capabilities of the controlled system confirming its effective performance with a THD of 3.77%, which respects the standard norms (the Australian standard (AS-4777-2005) and IEEE 929-2000 standard (IEEE-929-2000)). In addition to that, Fig. 7 displays the power generated by the PVs and the electrical grid to be absorbed by the nonlinear load. It is shown that when the PVs are unable to fully power the nonlinear load, the utility grid intervenes and provides the necessary power, thereby maintaining the power conservation principle.

## V. CONCLUSIONS

This paper has been devoted to the control of a PV-fed active power filter based on a cascaded H-bridge multilevel inverter. The design of the controller combines the sliding mode control and Lyapunov theory. The developed multi-loop regulator has successfully proven the efficiency of the chosen control techniques in achieving the desired objectives when it comes to the extraction of the maximum available PV power, dc link regulation, power factor correction, and harmonics compensation. The main aims behind using such structure are for its ability to empower the complete filtering chain, compensate the reactive and harmonics powers, and operate under faulty conditions. It has been demonstrated that all the control objectives have been met under different testing modes, which include matching and mismatching irradiations, in addition to faulty modes.

## REFERENCES


[1] L. Morán, J. Dixon, and M. Torres, Active Power Filters, in Power Electronics Handbook, Elsevier, pp. 1341-1379, 2018, doi: 10.1016/B978-0-12-811407-0.00046-5.

[2] Renault Alfredo, Pacher Julio, Comparatore Leonardo, Ayala Magno, Rodas Jorge, Gregor Raul, "MPC with Space Vector Phase-Shift PWM (SV-PSPWM) Technique with Harmonic Mitigation Strategy for Shunt Active Power Filters Based on H-Bridge Multilevel Converter," Frontiers in Energy Research, vol. 10, 2022, doi: 10.3389/fenrg.2022.779108.

[3] Xing Liu, Lin Qiu, Wenjie Wu, Jien Ma, Youtong Fang, Zhouhua Peng, Dan Wang, "Efficient model-free predictive power control for active front-end modular multilevel converter," International Journal of Electrical Power Energy Systems, vol 132, 2021, doi: j.ijepes.2021.107058.

[4] Liu, H., Ma, L., Song, W., Zhu, J., Peng, L., "A whole control strategy for cascaded H-bridge rectifiers under distorted grid voltage and unbalanced load," IET Power Electron., vol 00, pp. 1-13, 2023, doi: pel2.12454.

[5] J. Vaquero, N. Vázquez, I. Soriano, and J. Vázquez, "Grid-Connected Photovoltaic System with Active Power Filtering Functionality," International Journal of Photoenergy, vol. 2018, pp. 1-9, 2018, doi: 10.1155/2018/2140797.

[6] Villanueva, E., Correa, P., Rodríguez, J., Pacas, M., "Control of a single-phase cascaded H-bridge multilevel inverter for grid-connected photovoltaic systems," IEEE Transactions on industrial electronics, vol. 56, no. 11, pp. 4399-4406, 2009, doi: TIE.2009.2029579.

[7] T. He, M. Wu, D. D. -C. Lu, K. Song and J. Zhu, "Model Predictive Sliding Control for Cascaded H-Bridge Multilevel Converters With Dynamic Current Reference Tracking," in IEEE Journal of Emerging and Selected Topics in Power Electronics, vol. 10, no. 2, pp. 1409-1421, 2022, doi: JESTPE.2021.3053300.

[8] Andres A. Valdez-Fernandez, Gerardo Escobar, Daniel U. Campos-Delgado, Moises E. Hernandez-Ruiz, "Model-based control strategy for the three-phase n-level CHB multilevel converter," International Journal of Electrical Power Energy Systems, vol. 147, 2023, doi: j.ijepes.2022.108883.

[9] H. Katir, A. Abouloifa, K. Noussi, I. Lachkar and F. Giri, "Cascaded H-Bridge Inverters for UPS Applications: Adaptive Backstepping Control and Formal Stability Analysis," in IEEE Control Systems Letters, vol. 6, pp. 145-150, 2022, doi: 10.1109/LCSYS.2021.3051875.

[10] M. N. Musarrat, A. Fekih, M. A. Rahman, M. R. Islam and K. M. Muttaqi, "Event-triggered SMC-based FRT Approach for DFIG-based Wind Turbines Equipped with DVR with High Frequency Isolation," in IEEE Journal of Emerging and Selected Topics in Power Electronics, 2022, doi: JESTPE.2022.3233349.

[11] Wang, H., Ghaffari, V., Mobayen, S., Bartoszewicz, A., Fekih, A., Assawinchaichote, W., "Finite-time robust performance improvement for non-linear systems in the presence of input non-linearity and external disturbance. IET Control Theory Appl.," vol. 17, pp. 672–682, 2023, doi: cth2.12387

[12] H. Katir et al., "Fault Tolerant Backstepping Control for Double-Stage Grid-Connected Photovoltaic Systems Using Cascaded H-Bridge Multilevel Inverters," in IEEE Control Systems Letters, vol. 6, pp. 1406-1411, 2022, doi: 10.1109/LCSYS.2021.3095107.

[13] J.-J. E. Slotine and W. Li, Applied nonlinear control. Englewood Cliffs, N.J: Prentice Hall, 1991.

[14] A. Abouloifa, C. Aouadi, I. Lachkar, Y. Boussairi, M. Aourir, and A. Hamdoun, "Output-Feedback Nonlinear Adaptive Control Strategy of the Single-Phase Grid-Connected Photovoltaic System," Journal of Solar Energy, vol. 2018, pp. 1-14, 2018, doi: 10.1155/2018/6791056.